HHS Public Access

Author manuscript

Eur Radiol. Author manuscript; available in PMC 2023 October 01.

Ultra-high-resolution imaging of the shoulder and pelvis using photon-counting detector CT: A feasibility study in patients

Francis Baffour, MD[1,*], **Kishore Rajendran, PhD**[1,*], **Katrina N. Glazebrook, MD**[1], **Jamison E. Thorne, BS**[1], **Nicholas B. Larson, PhD**[2], **Shuai Leng, PhD**[1], **Cynthia H. McCollough, PhD**[1], **Joel G. Fletcher, MD**[1]

[1]Department of Radiology, Mayo Clinic, Rochester, MN, USA

[2]Department of Quantitative Health Sciences, Mayo Clinic, Rochester, MN, USA

Abstract

Objective: To evaluate ultra-high-resolution (UHR) imaging of large joints using an investigational photon-counting detector (PCD) CT.

Materials and Methods: Patients undergoing clinical shoulder or pelvis energy-integrating-detector (EID) CT exam were scanned using the UHR mode of the PCD-CT system. Axial EID-CT images (1-mm sections) and PCD-CT images (0.6-mm sections) were reconstructed using Br62/Br64, and Br76 kernels, respectively. Two musculoskeletal radiologists rated visualization of anatomic structures using a 5-point Likert scale. Wilcoxon rank-sum test was used for statistical analysis of reader scores, and paired t-test was used for comparing bone CT numbers and image noise from PCD-CT and EID-CT.

Results: Thirty-two patients (17 shoulders and 15 pelvis) were prospectively recruited for this feasibility study. Mean age for shoulder exams was 67.3 ± 15.5 years (11 females) and 47.2 ± 15.8 years (11 females) for pelvis exams. The mean volume CT dose-index was lower on PCD-CT compared to EID-CT (shoulders: 18 mGy vs. 34 mGy, pelvis: 11.6 mGy vs. 16.7 mGy). PCD-CT was rated significantly better than EID-CT ($p < 0.001$) for anatomic-structure visualization. Trabecular delineation in shoulders (mean score = 4.24 ± 0.73) and femoroacetabular joint visualization in the pelvis (mean score = 3.67 ± 1.03) received the highest scores. PCD-CT demonstrated significant increase in bone CT number ($p < 0.001$) relative to EID-CT; no significant difference in image noise was found between PCD-CT and EID-CT.

Conclusion: The evaluated PCD-CT system provided improved visualization of osseous structures in the shoulders and pelvises at a 31-47% lower radiation dose compared to EID-CT.

Keywords

X-Ray Computed Tomography; Shoulder; Pelvis; Hip joint; Radiation Dosage

Corresponding Author: Kishore Rajendran, PhD, Mayo Clinic, 200 First Street SW, Rochester, MN 55905 USA, Rajendran.Kishore@mayo.edu, Phone: 507-284-1765, Fax: 507-266-3661.

*both authors contributed equally to this work

1. Introduction

Most modern CT systems employ detector pixels of size range 0.5 - 0.625 mm [1]. To achieve further improvement in spatial resolution, smaller detector pixels are required. One method to achieve this in conventional energy-integrating detector (EID)-CT systems is to place an attenuating “comb” filter in front of the detector array to reduce the effective pixel aperture [2; 3]. Additionally, EIDs require reflective septa between detector elements to mitigate the spread of visible light that is created during the x-ray detection (scintillation). Both the comb filter and finite septae reduce geometric dose efficiency. Since the comb filter blocks x-rays after they have interacted with the patient resulting in increased image noise, higher doses are required. This limits the use of comb-filter technique to extremities (hand, elbow, knee, and ankle) and the temporal bone. Recently, ultra-high-resolution (UHR) imaging without the use of comb filters has become available in an EID-CT system which uses a 0.25 mm detector pixel (at isocenter) and very thin interpixel septae [4; 5].

Photon-counting detectors (PCD) achieve improved spatial resolution by use of smaller detector pixels. They do not require reflective septa or comb-filters as x-ray photons are directly converted to electrical pulses for digital readout, without the intermediate scintillation step used in EIDs [6-9]. Investigational PCD-CT systems capable of whole-body imaging have been reported in the literature with typical detector pixel sizes ranging from 0.20-0.27 mm [7; 10-15] and in-plane spatial resolution of 125-150 μm [13; 14; 16-19].

In this study, we report imaging of large joints (shoulders and pelvis) using an investigational PCD-CT system (SOMATOM Count Plus, Siemens Healthineers GmbH) with a 50 cm scan field-of-view (FOV). This system is equipped with small detector pixels of size 0.151 mm × 0.176 mm (at isocenter) in ultra-high resolution (UHR) mode [14]. To the best of our knowledge, PCD-CT imaging of large joints using a full-FOV scanner, and its potential benefits have not been previously reported. Our aim was therefore to evaluate improvements in anatomic structure visualization in shoulders and pelvises using the UHR mode of the PCD-CT system without a radiation dose penalty compared to conventional EID-CT.

2. Methods

2.1 Patient Data Collection

This prospective study was approved by our institutional review board. Signed informed consent was obtained from each participant. Between 11/23/2020 and 04/16/2021, patients 18 years and older scheduled to have a clinically indicated CT scan of the shoulder or pelvis were recruited to undergo the same exam on a research whole-body PCD-CT system. Pregnant patients, minors, and patients with metal implants were excluded from the study.

2.2 CT Image Acquisition and Reconstruction

Patients were first scanned on an EID-CT scanner (SOMATOM Force or Definition Edge+; Siemens Healthineers GmbH) using our routine clinical protocol. Immediately following their clinical EID-CT examinations, the research scan on the PCD-CT system (SOMATOM Count Plus) was performed (see Table 1). The PCD-CT scans using HR mode employed a

smaller focal spot (0.6 mm x 0.7 mm) compared to the EID-CT scans with the standard focal spot size (0.8 mm x 1.1 mm). Since the PCD-CT scan was performed using the UHR mode, a dedicated UHR body sharp kernel (Br76, cut-off frequency = 28 cm^{-1}) available only on the PCD-CT system was used for image reconstruction.

2.3 Image Review

Images were displayed on a dual-monitor clinical workstation and two fellowship-trained musculoskeletal radiologists with 28 and 7 years (K.N.G. and F.B.) of experience independently evaluated the images.

Images from each scanner type were randomly displayed on the left or right monitor for each subject and the readers were blinded to the scanner type, reconstruction settings and CT acquisition details. Since the cohort was not prescreened for specific pathologies, the readers were asked to examine the images with specific attention to anatomic structures that radiologists typically evaluate during routine assessment of shoulders and pelvises. Specifically, in each shoulder, the glenohumeral joint, humeral head, proximal humeral tuberosities, coracoid process, acromioclavicular joint, cortex and trabeculae were evaluated. For each pelvis, the femoroacetabular joints, femoral heads, femoral trochanters, ischial tuberosities, cortex, and trabeculae were evaluated. For this subjective assessment, readers were asked to examine the anatomic structures for visualization and diagnostic confidence. Osseous structures visualized on the images on the left monitor were scored relative to images on the right monitor using a 5-point Likert scale, (1- worse visualization and poor diagnostic confidence; 2 - worse visualization, no change in the diagnostic confidence; 3 - comparable visualization and similar diagnostic confidence; 4 - improved visualization and similar diagnostic confidence; 5 - improved visualization and improved diagnostic confidence). A post-hoc re-assignment of reader scores was performed such that the final scores reflected the performance of PCD-CT relative to that of EID-CT.

2.4 Objective image quality assessment

Mean CT numbers and image noise (standard deviation of CT numbers) were measured in circular region-of-interests (ROIs) placed in cortical bone and soft tissue (muscle), respectively. For the shoulders, ROIs of approximate area 1 mm^2 and 78 mm^2 were placed in proximal humeral diaphyseal cortex and surrounding soft tissue, respectively. For the pelvises, ROIs of approximate area 13 mm^2 and 282 mm^2 were placed in the proximal femoral diaphyseal cortex and surrounding soft tissue, respectively. ROIs sizes were matched between EID-CT and PCD-CT measurements.

2.5 Statistical analysis

A one-sample Wilcoxon rank-sum test was used to test for significant asymmetry of Likert scores about the null value of 3 using the mean scores between readers, and a p-value < 0.05 was considered statistically significant under a two-sided alternative. Testing was performed for each individual anatomical structure. Median, mean, and standard deviations (SDs) of scores for each structure are recorded individually. Inter-reader agreement was calculated using Cohen's Kappa (κ) using quadratic weights. Agreements were interpreted using the following Kappa scale: no agreement ($\kappa \leq 0$), slight agreement ($0 < \kappa \leq 0.20$), fair ($0.20 < \kappa$

≤ 0.40), moderate (0.40 < κ ≤ 0.60), substantial (0.60 < κ ≤ 0.80), and perfect agreement (κ > 0.80). For objective image quality, bone CT number and image noise measurements were compared using student t-test and a p-value < 0.05 was considered statistically significant.

3. Results

3.1 Patient population

Thirty-two patients were included in this study comprising of 10 males and 22 females. Seventeen of these patients underwent a shoulder CT (mean age 67.3 ± 15.5 years, 11 were female) and fifteen patients underwent pelvis CT (mean age 47.2 ± 15.8 years, 11 were female).

3.2 Comparison between EID-CT and PCD-CT of the Shoulder

The mean CTDIvol was 47% lower on PCD-CT (18 mGy) compared to EID-CT (33.8 mGy). The PCD-CT images were rated significantly better than EID-CT by both readers for the evaluated structures in the shoulders ($p < 0.001$, Table 2). The median score for PCD-CT from the two readers was 4 for each structure. Trabecular delineation received the highest overall score (reader-1 mean score = 4.12 ± 0.93 and reader-2 mean score = 4.35 ± 0.49). Slight agreement was observed between the two readers (average κ = 0.08 ± 0.08, see supplemental information for individual κ values).

Figure 1 shows PCD-CT and EID-CT images from a 52-year-old female with an ununited fracture through the base of the coracoid process. Figure 2 shows PCD-CT and EID-CT images from a 33-year-old male with a healing fracture through the glenoid. Early callus formation at the base of the fracture (yellow arrows) is more conspicuous on the PCD-CT image compared to EID-CT. Figure 3 shows CT images from a 72-year-old male with suspected osteoarthritis where PCD-CT better demonstrates intraarticular gas.

3.3 Comparison between EID-CT and PCD-CT of the Pelvis

The mean CTDIvol was 31% lower on PCD-CT (11.6 mGy) compared to EID-CT (16.7 mGy). PCD-CT images were rated significantly better than EID-CT by both readers for the evaluated pelvic structures ($p < 0.05$, Table 3). The median score for PCD-CT from the two readers ranged between 3.5 and 4.0 for each structure. Femoroacetabular joint received the highest overall score (reader-1 mean score = 3.53 ± 0.64 and reader-2 mean score = 3.80 ± 1.32). Substantial agreement was observed between the two readers scores (average κ = 0.61 ± 0.14, see supplemental information for individual κ values).

Figure 4 shows PCD-CT and EID-CT images from a 54-year-old male with degenerative arthritis in both hips. There is improved visualization of trabeculae on the PCD-CT image, leading to clearer margins of the bone islands in the left femoral head.

3.4 Objective image quality evaluation

Mean CT numbers measured from cortical bone and image noise measured from soft tissue region are plotted in Figure 5. Bone CT number from PCD-CT was significantly higher (p

< 0.001) compared to EID-CT, while no significant difference in image noise was found between PCD-CT and EID-CT for both shoulder and pelvis images.

4. Discussion

This study sought to evaluate the effect of improved spatial resolution facilitated by PCD technology for imaging of shoulder and pelvic joints. UHR images from PCD-CT were preferred by radiologists for anatomic structure visualization relative to conventional EID-CT, despite a 31-47% reduction in radiation dose. Specifically, the fine cortical and trabecular detail in the shoulders and pelvises were identified with greater confidence in the PCD-CT UHR images. The presence and absence of bridging callus (Figures 2 and 1, respectively) along the margins of healing bone were more confidently identified on PCD-CT, and sequalae of hypertrophic degenerative arthritis such as marginal osteophytes and physiologic intraarticular gas (Figure 3) were clearly depicted on PCD-CT UHR images. Objective image quality evaluation showed a statistically significant increase in cortical bone CT numbers from PCD-CT images relative to EID-CT, while no significant difference in image noise was observed between EID-CT and PCD-CT.

Resolving sub-millimeter structures in musculoskeletal joints increases diagnostic confidence for detection of osseous pathology. The resolution achievable using comb filters on some EID-CT systems has not been employed for large joints due to the radiation dose penalty associated with the use of attenuating filters [20-23]. Alternatively, improved spatial resolution in CT of large joints is typically achieved by use of sharper reconstruction kernels (to resolve higher spatial frequencies) and/or with thinner slices (to reduce partial volume averaging). The PCD-CT system used in our study features a detector pixel size of 0.15 mm x 0.176 mm at isocenter with an effective nominal slice thickness of 0.2 mm. This system has been reported to yield a limiting in-plane resolution of 125 microns with dedicated sharp kernels [14]. The geometric dose efficiency of PCDs is intrinsically high due to the absence of interpixel septae [24]. Consequently, the small-pixel PCD design mitigates the need for attenuating comb filter to achieve high spatial resolution. PCDs provide additional benefits such as higher contrast-to-noise ratio by uniform weighting of x-ray photons irrespective of their energy [25] and removal of electronic noise from the detected signal by energy thresholding [9] compared to EID-CT.

The 50-cm FOV in this investigational PCD-CT system (vs. 27.5 cm FOV in the previous research system from the same manufacturer, SOMATOM CounT) allows for bilateral imaging of large joints at clinical dose levels and dose rates. This previously reported system lacked automatic tube current modulation in the angular direction. This feature is particularly crucial for imaging of shoulders, where the lateral patient size is relatively large compared to the anteroposterior patient size. The PCD-CT system evaluated in our current study featured tube current modulation control in both longitudinal and angular directions (CARE Dose4D, Siemens Healthineers GmbH) similar to clinical scanners from the same manufacturer, which served to decrease lateral streaking artifacts and yielded more uniform noise texture. The 0.15 mm × 0.176 mm detector pixel size and the intrinsic system spatial resolution are identical to the recently introduced clinical PCD-CT system [26].

Our study had the following limitations. First, due to the investigational nature of the scanner, metal artifact reduction software was not available on the PCD-CT system; patients with metal implants were therefore excluded from participation in the study. The total cohort size of 32 was deemed sufficient for our feasibility study to evaluate the benefits of improved spatial resolution and dose reduction of this PCD-CT system for imaging of large joints. Studies focusing on specific musculoskeletal pathology in larger cohorts may further elucidate specific diagnostic benefits of PCD technology. The PCD-CT system allows thinner sections (0.2 mm) and sharper kernels [14] (with cut-off spatial frequencies up to 40 cm^{-1}) than those used in our study. The dose reduction factor (determined by image noise level) from the PCD-CT system progressively decreases with increasing kernel sharpness and/or decreasing section thickness. Therefore, as a tradeoff between spatial resolution improvement and dose reduction, we used a Br76 kernel (cut-off spatial frequency of 28 cm^{-1}) for PCD-CT reconstructions, while simultaneously achieving 31-47% dose reduction. Further reduction in radiation dose could be achieved using tin prefiltration as demonstrated in other studies[18; 27]; tin filter was not available on the PCD-CT system used in our study at the time of this investigation. For further improvements in spatial resolution for visualization of bone detail, dedicated ultra-high-resolution kernels (e.g., Br98) and/or thinner sections can be employed [28]. At present, the evaluated PCD-CT system uses one energy threshold in the UHR mode; however, this is not a fundamental limitation of PCD technology. The PCD array can enable up to four energy thresholds per detector pixel when fully configured [14; 29], which could potentially be used for simultaneous UHR and multi-energy imaging of joints. For instance, virtual non-calcium images at high spatial resolution or low image noise could be used to evaluate bone marrow edema or virtual monoenergetic images at higher photon energy (keV) could be used in tandem with metal artifact reduction software to mitigate severe artifacts from metal hardware. Additional studies are warranted to evaluate such uses in systems with higher data transfer rates that allow simultaneous UHR and multi-energy imaging.

In conclusion, we demonstrated ultra-high-resolution imaging of large joints using a full-FOV PCD-CT system. Reader scores for each of the evaluated critical structures showed PCD-CT images to be significantly better than EID-CT images for visualization of critical osseous structures even though were acquired using 31- 47% less radiation dose.

Supplementary Material

Refer to Web version on PubMed Central for supplementary material.

Abbreviations

EID	Energy-integrating detector
PCD	Photon-counting detector
UHR	Ultra-high resolution
FOV	Field of view
ROI	Region of interest

SD	Standard deviation

References

1. Wang J, Fleischmann D (2018) Improving Spatial Resolution at CT: Development, Benefits, and Pitfalls. Radiology 289:261–262 [PubMed: 29944083]
2. Flohr TG, Stierstorfer K, Suss C, Schmidt B, Primak AN, McCollough CH (2007) Novel ultrahigh resolution data acquisition and image reconstruction for multi-detector row CT. Med Phys 34:1712–1723 [PubMed: 17555253]
3. Leng S, Diehn FE, Lane JI et al. (2015) Temporal Bone CT: Improved Image Quality and Potential for Decreased Radiation Dose Using an Ultra-High-Resolution Scan Mode with an Iterative Reconstruction Algorithm. AJNR Am J Neuroradiol 36:1599–1603 [PubMed: 25999413]
4. Kakinuma R, Moriyama N, Muramatsu Y et al. (2015) Ultra-High-Resolution Computed Tomography of the Lung: Image Quality of a Prototype Scanner. PLoS One 10:e0137165 [PubMed: 26352144]
5. Oostveen LJ, Boedeker KL, Brink M, Prokop M, de Lange F, Sechopoulos I (2020) Physical evaluation of an ultra-high-resolution CT scanner. Eur Radiol 30:2552–2560 [PubMed: 32040726]
6. Hsieh SS, Leng S, Rajendran K, Tao S, McCollough CH (2021) Photon Counting CT: Clinical Applications and Future Developments. IEEE Transactions on Radiation and Plasma Medical Sciences 5:441–452 [PubMed: 34485784]
7. Leng S, Yu Z, Halaweish A et al. (2016) Dose-efficient ultrahigh-resolution scan mode using a photon counting detector computed tomography system. J Med Imaging (Bellingham) 3:043504 [PubMed: 28042589]
8. Pourmorteza A, Symons R, Henning A, Ulzheimer S, Bluemke DA (2018) Dose Efficiency of Quarter-Millimeter Photon-Counting Computed Tomography: First-in-Human Results. Invest Radiol 53:365–372 [PubMed: 29595753]
9. Willemink MJ, Persson M, Pourmorteza A, Pelc NJ, Fleischmann D (2018) Photon-counting CT: Technical Principles and Clinical Prospects. Radiology 289:293–312 [PubMed: 30179101]
10. Boccalini S, Si-Mohamed S, Dessouky R, Sigovan M, Boussel L, Douek P (2021) Feasibility of human vascular imaging of the neck with a large field-of-view spectral photon-counting CT system. Diagn Interv Imaging. 10.1016/j.diii.2020.12.004
11. da Silva J, Gronberg F, Cederstrom B et al. (2019) Resolution characterization of a silicon-based, photon-counting computed tomography prototype capable of patient scanning. J Med Imaging (Bellingham) 6:043502 [PubMed: 31620547]
12. Euler A, Higashigaito K, Mergen V et al. (2021) High-Pitch Photon-Counting Detector Computed Tomography Angiography of the Aorta: Intraindividual Comparison to Energy-Integrating Detector Computed Tomography at Equal Radiation Dose. Invest Radiol. 10.1097/RLI.0000000000000816
13. Ferda J, Vendis T, Flohr T et al. (2021) Computed tomography with a full FOV photon-counting detector in a clinical setting, the first experience. Eur J Radiol 137:109614 [PubMed: 33657475]
14. Rajendran K, Petersilka M, Henning A et al. (2021) Full field-of-view, high-resolution, photon-counting detector CT: technical assessment and initial patient experience. Phys Med Biol. 10.1088/1361-6560/ac155e
15. Si-Mohamed S, Boccalini S, Rodesch PA et al. (2021) Feasibility of lung imaging with a large field-of-view spectral photon-counting CT system. Diagn Interv Imaging 102:305–312 [PubMed: 33610503]
16. Bartlett DJ, Koo CW, Bartholmai BJ et al. (2019) High-Resolution Chest Computed Tomography Imaging of the Lungs: Impact of 1024 Matrix Reconstruction and Photon-Counting Detector Computed Tomography. Invest Radiol 54:129–137 [PubMed: 30461437]
17. Leng S, Rajendran K, Gong H et al. (2018) 150-μm Spatial Resolution Using Photon-Counting Detector Computed Tomography Technology: Technical Performance and First Patient Images. Invest Radiol. 10.1097/RLI.0000000000000488

18. Rajendran K, Voss BA, Zhou W et al. (2020) Dose Reduction for Sinus and Temporal Bone Imaging Using Photon-Counting Detector CT With an Additional Tin Filter. Invest Radiol 55:91–100 [PubMed: 31770297]
19. Wehrse E, Sawall S, Klein L et al. (2021) Potential of ultra-high-resolution photon-counting CT of bone metastases: initial experiences in breast cancer patients. NPJ Breast Cancer 7:3 [PubMed: 33398008]
20. Erickson SJ (1997) High-resolution imaging of the musculoskeletal system. Radiology 205:593–618 [PubMed: 9393511]
21. Krahe T, Nicolas V, Ring S, Warmuth-Metz M, Koster O (1989) [Diagnostic evaluation of full x-ray pictures and computed tomography of bone tumors of the spine]. Rofo 150:13–19 [PubMed: 2536490]
22. Helms CA, Cann CE, Brunelle FO, Gilula LA, Chafetz N, Genant HK (1981) Detection of bone-marrow metastases using quantitative computed tomography. Radiology 140:745–750 [PubMed: 7280245]
23. Krestan CR, Noske H, Vasilevska V et al. (2006) MDCT versus digital radiography in the evaluation of bone healing in orthopedic patients. AJR Am J Roentgenol 186:1754–1760 [PubMed: 16714670]
24. Danielsson M, Persson M, Sjolin M (2021) Photon-counting x-ray detectors for CT. Phys Med Biol 66:03TR01
25. Gutjahr R, Halaweish AF, Yu Z et al. (2016) Human Imaging With Photon Counting-Based Computed Tomography at Clinical Dose Levels: Contrast-to-Noise Ratio and Cadaver Studies. Investigative radiology. 10.1097/RLI.0000000000000251
26. Rajendran K, Petersilka M, Henning A et al. (2022) First Clinical Photon-counting Detector CT System: Technical Evaluation. Radiology. 10.1148/radiol.212579:212579
27. Stern C, Sommer S, Germann C et al. (2021) Pelvic bone CT: can tin-filtered ultra-low-dose CT and virtual radiographs be used as alternative for standard CT and digital radiographs? Eur Radiol 31:6793–6801 [PubMed: 33710371]
28. Bette SJ, Braun FM, Haerting M et al. (2021) Visualization of bone details in a novel photon-counting dual-source CT scanner-comparison with energy-integrating CT. Eur Radiol. 10.1007/s00330-021-08441-4
29. Flohr T, Petersilka M, Henning A, Ulzheimer S, Ferda J, Schmidt B (2020) Photon-counting CT review. Phys Med 79:126–136 [PubMed: 33249223]

Key points:

1. A full field-of-view PCD-CT with 0.15 mm x 0.176 mm detector pixel size (isocenter) facilitates bilateral, high-resolution imaging of shoulders and pelvis.
2. The evaluated investigational PCD-CT system was rated superior by two musculoskeletal radiologists for anatomic structure visualization in shoulders and pelvises despite a 31-47% lower radiation dose compared to EID-CT.
3. PCD-CT demonstrated significantly higher bone CT number compared to EID-CT, while no significant difference in image noise was observed between PCD-CT and EID-CT.

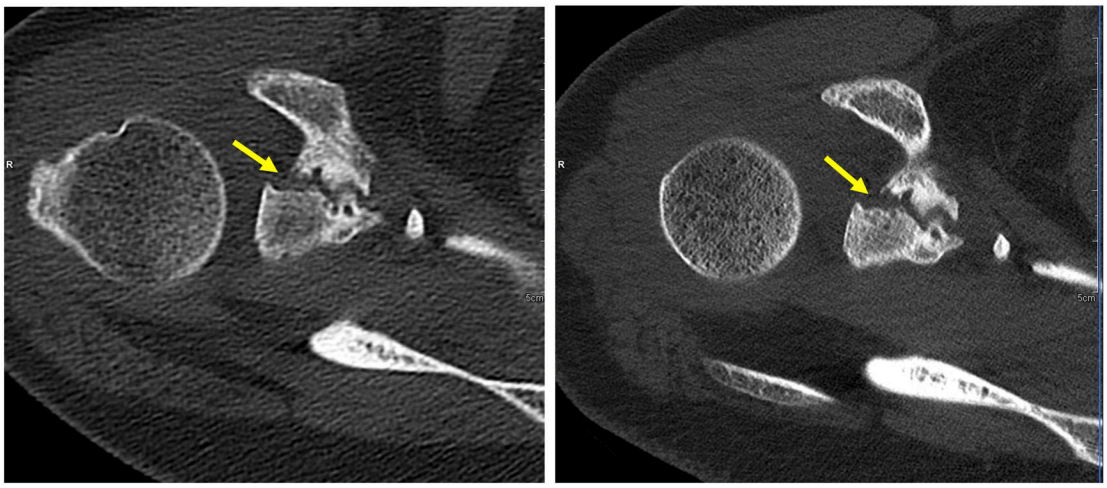

Figure 1:
EID-CT (left) and PCD-CT (right) images from a patient with an ununited glenoid fracture through the base of coracoid process. There is no bridging bone or callus at the fracture margins (arrows). This is more apparent on the PCD-CT image.

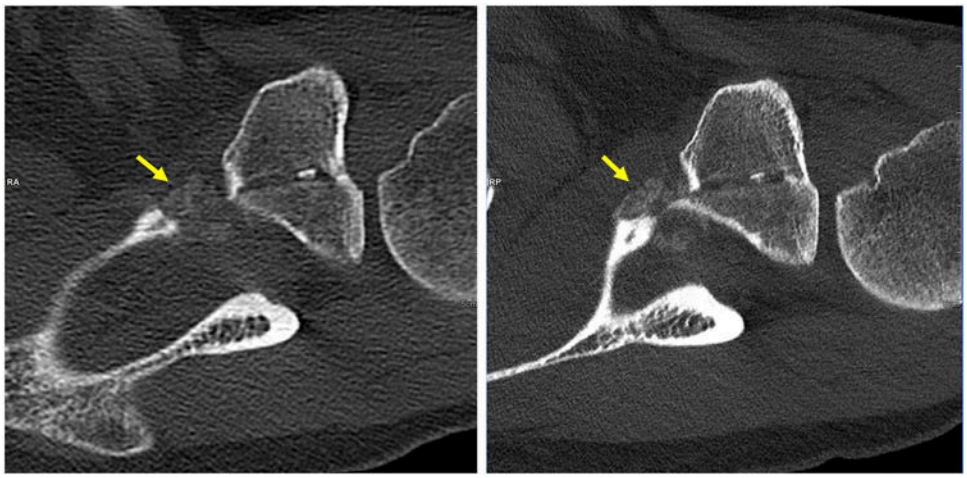

Figure 2:
EID-CT and PCD-CT images of a patient with a healing fracture of the glenoid. Early callus formation at the base of the fracture (marked by arrows) is more conspicuous on the PCD image.

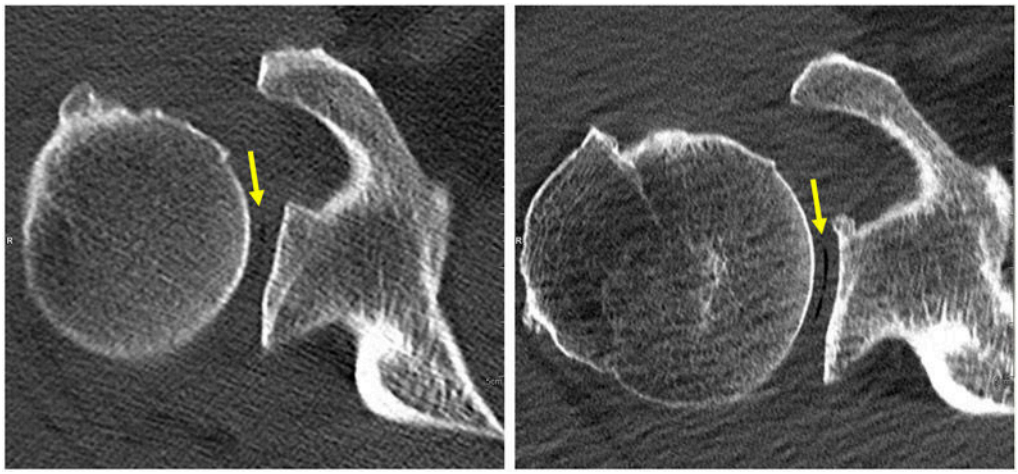

Figure 3:
EID-CT (left) and PCD-CT (right) images of a patient with intraarticular gas in the glenohumeral joint related to vacuum phenomenon. The intraarticular gas is more clearly visualized on the PCD-CT image compared to EID-CT.

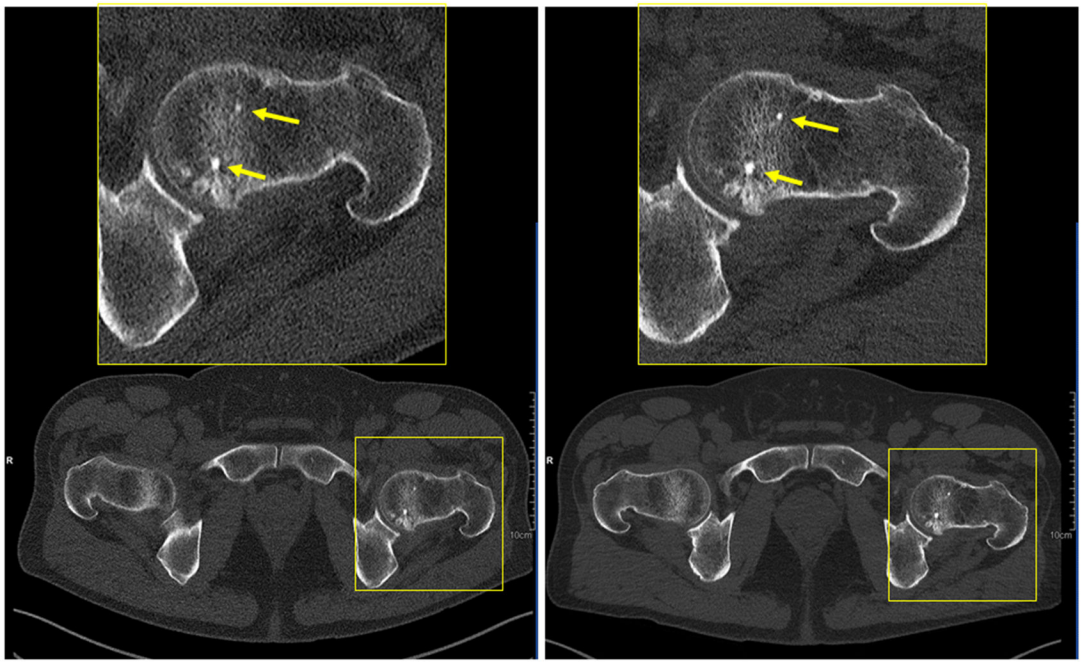

Figure 4:
EID-CT (left) and PCD-CT (right) images of a patient with degenerative arthritis in both hips. Improved conspicuity of trabeculae and bone islands (marked by arrows) in the femoral head (enlarged view in top row) can be seen in the PCD-CT image.

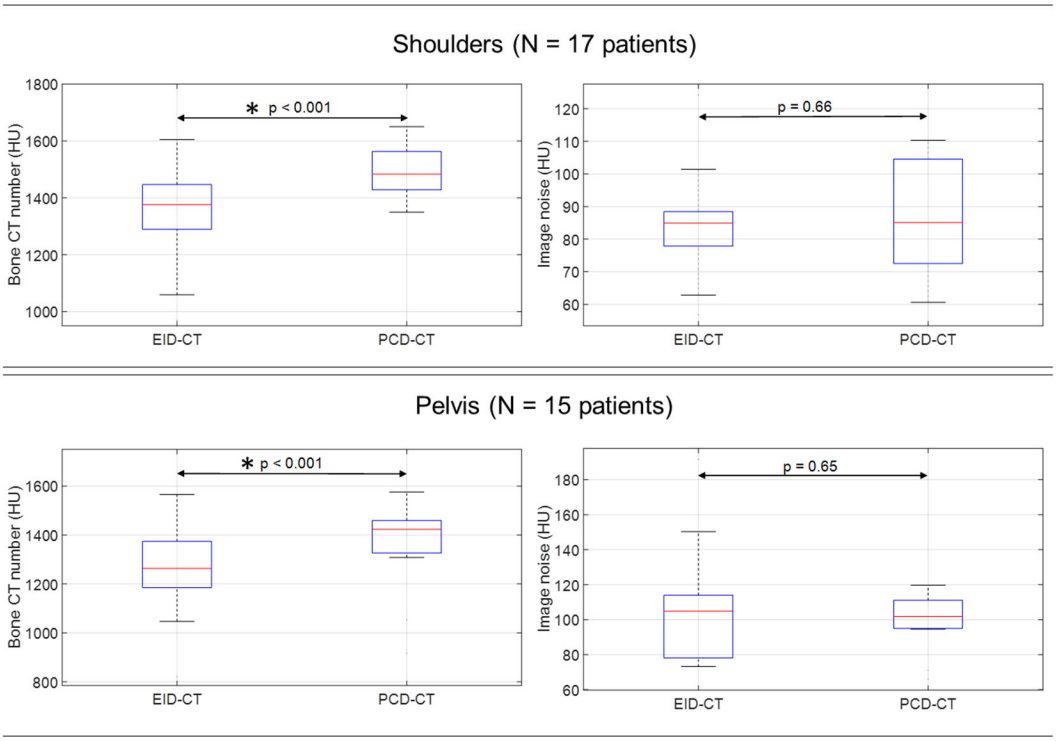

Figure 5:

Cortical bone CT number and image noise (standard deviation measured in muscle) measurements for EID-CT and PCD-CT in the shoulder and hip cohorts. The red horizontal lines in the box plots indicate the median values. In both cohorts, PCD-CT showed significant increase in bone CT number ($p < 0.001$ indicated by * in the plots, paired t-test) compared to EID-CT. No significant differences in image noise were found between EID-CT and PCD-CT.

Table 1:

CT acquisition and reconstruction parameters

	Shoulder		Pelvis	
	EID-CT	**PCD-CT**	**EID-CT**	**PCD-CT**
Scanner model	SOMATOM Force (or) Definition Edge+	SOMATOM Count Plus	SOMATOM Force (or) Definition Edge+	SOMATOM Count Plus
Collimation	192 x 0.6 mm (Force) 128 x 0.6 mm (Edge+)	120 x 0.2 mm	192 x 0.6 mm (Force) 128 x 0.6 mm (Edge+)	120 x 0.2 mm
Tube potential (kV)	140	140	120 or 140	120 or 140
Automatic tube current modulation	ON[1]	ON[1]	ON[1]	ON[1]
CTDIvol: Mean ± SD(32 cm)	33.8 ± 12.9	18.05 ± 6.4	16.7 ± 12.3	11.6 ± 3.9
Reconstruction kernel	Br64 (Force) Br62 (Edge+)	Br76	Br64 (Force) Br62 (Edge+)	Br76
Reconstruction technique	Iterative reconstruction (ADMIRE, strength 2)	Iterative reconstruction (PNR, strength 3)	Iterative reconstruction (ADMIRE, strength 2)	Iterative reconstruction (PNR, strength 3)
Slice thickness	1.0 mm	0.6 mm	1.0 mm	0.6 mm
Image matrix size	1024 x 1024	1024 x 1024	1024 x 1024	1024 x 1024

EID: Energy-integrating detector; PCD: Photon-counting detector; CTDIvol: Volume CT dose index; SD: Standard deviation; PNR: Prior-based Noise Reduction; ADMIRE: Advanced Modeled Iterative Reconstruction

[1]CARE Dose4D (Siemens Healthineers GmbH)

Table 2:

Reader scores for critical structure evaluation in the shoulders for PCD-CT relative to EID-CT

Shoulders	Median score (mean ± SD)	p-value*
Glenohumeral joint	4.00 (3.94±0.81)	< 0.001
Humeral head	4.00 (4.15±0.70)	< 0.001
Proximal humeral tuberosities	4.00 (3.62±0.65)	< 0.001
Coracoid process	4.00 (3.65±0.73)	< 0.001
Acromioclavicular joint	4.00 (3.65±0.77)	< 0.001
Cortex	4.00 (4.06±0.81)	< 0.001
Trabeculae	4.00 (4.24±0.73)	< 0.001

SD: standard deviation

*Wilcoxon rank-sum test

Table 3:

Reader scores for critical structure evaluation in the pelvises for PCD-CT relative to EID-CT

Pelvis	Median score (mean ± SD)	p-value*
Femoroacetabular joint	4.00 (3.67±1.03)	< 0.005
Femoral head	4.00 (3.63±1.13)	< 0.005
Femoral trochanters	3.50 (3.53±0.85)	< 0.005
Ischial tuberosity	4.00 (3.60±0.93)	< 0.005
Cortex	4.00 (3.57±1.14)	< 0.05
Trabeculae	3.50 (3.53±1.19)	< 0.05

SD: Standard deviation

*Wilcoxon rank-sum test